Available online at www.sciencedirect.com
ScienceDirect
Ceramics International 37 (2011) 1–8
CERAMICS INTERNATIONAL
www.elsevier.com/locate/ceramint

Mechanical properties of cBN–Al composite materials

Amanda McKie [a], Jami Winzer [b], Iakovos Sigalas [a,*], Mathias Herrmann [c], Ludwig Weiler [b], Jürgen Rödel [b], Nedret Can [d]

[a] School of Chemical and Metallurgical Engineering, University of the Witwatersrand, 2050 Johannesburg, South Africa
[b] Technische Universität Darmstadt, Institute of Materials Science, 64287 Darmstadt, Germany
[c] IKTS, Fraunhofer Institute for Ceramic Technology and Systems, 01277 Dresden, Germany
[d] Element Six (Pty) Ltd., Springs, South Africa

Received 31 March 2010; received in revised form 7 April 2010; accepted 30 May 2010
Available online 3 August 2010

Abstract

The relationship between microstructure and mechanical properties for a wide range of composite materials based on polycrystalline cubic boron nitride and aluminium as a binder phase (PcBN–Al) has been examined. The PcBN–Al composites were made using high-pressure, high-temperature (HPHT) sintering methods, yielding materials with grain sizes of cBN between 2 and 20 μm and an initial amount of Al binder between 15 and 25 vol.%. Hardness ranged between 15 and 40 GPa, while fracture toughness and strength were between 6.4–8.0 MPa $m^{1/2}$ and 355–454 MPa, respectively. Fractography was employed to investigate the large scatter in fracture strengths and correlate fracture strength with fracture toughness through the size of the fracture origins.

Keywords: C. Mechanical properties; C. Hardness; Polycrystalline cubic boron nitride (cBN); Fracture toughness; Bending strength

1. Introduction

Cubic boron nitride (cBN) has excellent physical properties, in particular high hardness of 50 GPa, second only to diamond, at 90 GPa [1,2]. Thus, it is widely used in cutting tool applications for hardened steels, cast iron and other ferrous alloys. Other properties of cBN include high thermal conductivity, and chemical and thermal stability, the latter two out ranking even diamond [1]. The development of cBN was motivated by the search for an alternative super-hard material to diamond, since diamond graphitizes when cutting ferrous materials, making it unsuitable for this application.

Sintering of cBN is difficult due to the predominantly covalent bonding [3]. Extremely high-pressures and -temperatures of 7.5–8 GPa and >2000 °C are required to obtain complete densification [4]. These conditions are not yet realistic on a large-scale industrial level [2]. The use of binders and high-pressure, high-temperature (HPHT) conditions is the method of choice for sintering cBN materials with temperatures and pressures in the range of 1200–1500 °C and 4–7 GPa, respectively [1]. Metals of the groups IV, V and VI of the periodic table or their compounds or other metallic elements such as aluminium, cobalt and nickel [5,6] are used as binders to aid sintering.

Wentorf and Rocco [7] first reported the synthesis of cBN with aluminium in 1972 using high-pressure high-temperature conditions. Walmsley and Lang investigated the commercial material Amborite (cBN–Al composite with a grain size of 8 μm, binder content 16–18%) in a transmission electron microscope (TEM) and found that Al had transformed to AlN and AlB_2 [8]. These phases hinder the conversion of cBN to hBN. Rong and Fukunaga later found the presence of a third phase, α-AlB_{12} [9]. Rapid grain growth of AlN and AlB_2 was observed during sintering thus lowering the mechanical properties [10]. In 2004 Rong further investigated this composite and found that AlN grains are always found around cBN grains, but did not find AlB_2 grains in contact with cBN [11]. Recently, Zhao conducted X-ray diffraction (XRD) analysis of the reaction between cBN and Al at different temperatures and the effect on final phase composition [12]. It was found that Al begins to react with cBN at 1400 °C and 5.5 GPa, with the formation of AlN and AlB_2 resulting. Li et al.

* Corresponding author.
E-mail address: Iakovos.sigalas@wits.ac.za (I. Sigalas).

0272-8842/$36.00
doi:10.1016/j.ceramint.2010.07.034

[13] investigated the sintering behavior of cBN–Al composites on WC-16 wt.% Co substrates. AlN and AlB_2 phases were detected and as seen by Rong and Yano [11] AlN was found to surround the cBN grains.

It is important to know the mechanical properties of polycrystalline cBN materials such as hardness, fracture toughness and fracture strength, σ_f, in order to fully understand the behavior of these materials in an application. There has not yet been an extensive mechanical testing study carried out on cBN–Al composites. Li et al. [13] reported hardness values of 20–32.7 GPa for 5–15 wt.% Al additives and showed that hardness increased with increasing cBN content. Benko et al. [10] reported a hardness value of 10 GPa before and 20 GPa after an extra annealing step. However, the sintering stage was only carried out at relatively low pressure of 10 MPa and 1750 °C. Wada and Yamashita [14] reported the microhardness of cBN–Al films formed by ion-beam assisted deposition to be 45–55 GPa.

In this work, the effect of mean grain size of cBN (2–20 μm) and Al content (15–25%) on hardness, fracture toughness and bending strength of cBN–Al composites is explored. The various compositions of the investigated materials are labeled according to the composition of the starting materials.

2. Experimental procedures

2.1. Sample preparation

The cBN–Al composites were made by powder processing followed by reaction sintering under high-pressure, high-temperature (HPHT) conditions. 10 compositions of the composite materials were made using various cBN powders of grain size ranging from 2 to 20 μm and initial amount of Al binder phase between 15 and 25 vol.%. Dry powder processing techniques were used over wet processing techniques as it would be necessary to use non-water-based milling fluids with surfactants and binding agents which would be impossible to burn-out prior to sintering. The correct weight proportions of cBN (supplied by Element Six (Pty) Ltd.) and aluminium (Supplied by Saarchem, 99.7%) powders were added together and mixed on a laboratory scale independent of industrial processes in a turbula mixer with steel balls of 10 mm in diameter for 1 h. Table 1 shows the various cBN composites prepared and the achieved densities. A nomenclature of the type G*x*cBN*y* was employed with *x* being the grain size of the boron nitride in microns and *y* the volume percent of aluminium added initially.

The mixed powder was then uniaxially compacted at 5 MPa into 50 mm diameter, 4 mm thickness disks and vacuum degassed to remove any gaseous impurities from the powder. The compacted powder pellets were then placed into capsules for sintering. The pellets were sintered under high-temperature and high-pressure conditions at 1400 °C and 5 GPa.

2.2. Materials characterization

Density measurements were done on the sintered composites using the Archimedes principle. The microstructure and phase content of the composites were analysed using scanning electron microscope (SEM) 'LEO1525FE', equipped with an energy dispersive spectroscopy detector (EDS) 'Oxford link Pentfet' and X-ray diffraction (XRD) 'Philips PW1710'. The amount of unreacted aluminium was determined using Rietveld refinement analysis using Topas A version 4.1 and structural models used were taken from the ICSD – version 1.4.4.

The grain size and binder content in the sintered materials were determined using polished cross-sections and quantitative image analysis of SEM-micrographs taken at a magnification of 5000 and 3000 times, respectively, for the G2 and G6, while G10 and G20 were taken at 1000 times. The cBN-particle size given in Table 1 is the equivalent circle diameter. The sintered binder content includes all phases besides the cBN phase, i.e. AlN, AlB_2 and unreacted Al if present.

2.3. Mechanical properties

The sintered samples were cut into required dimensions for characterization and mechanical properties testing. The specimens were subjected to hardness, bending strength and fracture toughness testing at room temperature.

Samples for characterization and hardness measurements were cut into 10 mm squares and polished to a mirror surface finish using a diamond wheel-polishing machine. Hardness

Table 1
Composition and density of cBN–Al composites.

Sample name	Starting cBN grain size (μm)	Starting Al binder content (vol.%)	Sintered cBN grain size (μm)	Sintered binder content (vol.%)	Density	
					(g/cm^3)	(%)
G2cBN15	2	15	1.5	17.9	3.360	99.2
G2cBN20	2	20	1.7	29.8	3.350	99.6
G2cBN25	2	25	1.8	40.0	3.345	99.6
G6cBN15	6	15	4.7	25.7	3.392	99.6
G6cBN20	6	20	4.7	32.0	3.356	99.5
G6cBN25	6	25	4.7	40.7	3.347	99.7
G10cBN15	12	15	10.8	19.3	3.388	99.5
G20cBN15	17	15	12.5	24.9	3.362	98.7
G20cBN20	17	20	13.2	29.5	3.358	99.5
G20cBN25	17	25	12.8	39.8	3.308	99.1

measurements were done using the Vickers hardness test method with a load of 49 N for 10 s. Samples were characterized using XRD and the microstructure was determined using SEM.

Fracture toughness [15] and strength [16] measurements were done in four-point bending configuration. Load and support spans were 10 and 20 mm, respectively. Specimen dimensions were $3\ mm^3 \times 4\ mm^3 \times 25\ mm^3$. For fracture toughness measurements the Single Edge V-notch Beam (SEVNB) method was used [15,17]. A V-notch was cut into the fracture toughness specimens using a 0.3 mm thick diamond saw for the first 800 μm and then a razor blade cutting machine with diamond paste for the final 200 μm. The notch depth was around 1 mm with a sharp V shaped notch radius of 10–30 μm. For strength tests the surfaces of the specimens were finished as recommended by EN 843-1 [18], the side edges were chamfered by 0.1 mm. The tests were performed on a universal servohydraulic testing machine MTS 810.22, 100 kN load frame, load cell 5 kN, with a cross-head speed of 5 μm/s, equivalent to ∼100 N/s or ∼40 MPa/s. For fracture toughness measurements 4–6 specimens were tested per material composition, for strength testing 20 samples per material composition.

For statistical analysis of strength data the Weibull distribution was applied. Their parameters, characteristic strength, σ_o, and Weibull modulus, m, were evaluated by the Maximum Likelihood method according to the European Standard EN 843-5 [19]. The 90% confidence intervals of σ_o and m were determined according to [20].

3. Results and discussion

3.1. Microstructure

Table 1 includes the composition and grain size of the cBN particles before and after sintering, and the density of the 10 cBN composite sample materials tested. The average grain size of the sintered cBN composite materials ranged between 1.5 and 14 μm. A decrease in the cBN grain size before and after sintering is due to the crushing during mixing and the reactive sintering of the materials. Density measurements showed that the materials were fully densified. Small variations in density can be caused by oxygen content and slightly different degrees of reaction.

The microstructures of the 15 and 25 vol.% Al sintered polycrystalline cBN–Al composites are provided in Fig. 1a–f. From XRD analysis of the cBN–Al composites it was found that the phases AlN and AlB_2 are present, consistent with [8]. Three materials were chosen to investigate for the small unreacted amounts of Al. In the following composites: G6cBN25, G20cBN20 and G20cBN25, the amount of residual Al was 1.8, 1.1 and 2.7 wt.%, respectively, suggesting that the degree of unreacted aluminium was small, in the order of 1–3 wt.% and is not expected to impact the mechanical properties noticeably. The SEM images show the microstructure of the cBN–Al composites. The dark phase is the cBN, the light grey phase is AlN, the darker grey phase is AlB_2 and the light phase is unreacted Al (see Fig. 2). Increasing the binder content and cBN grain size resulted in an increased amount of residual,

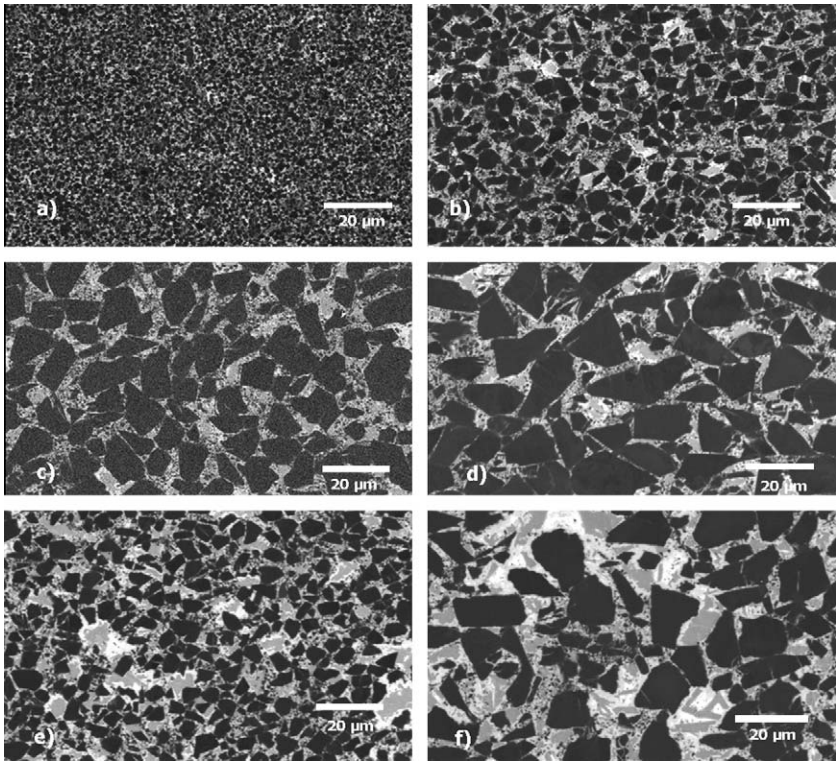

Fig. 1. Microstructure of the PcBN–Al composite materials: (a) G2cBN15, (b) G6cBN15, (c) G10cBN15, (d) G20cBN15, (e) G6cBN25 and (f) G20cBN25.

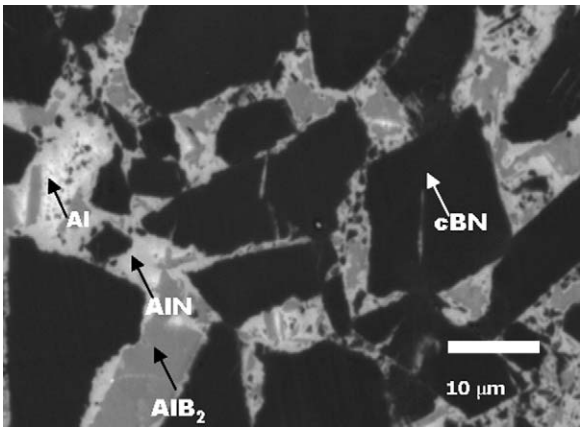

Fig. 2. Microstructure of G20cBN25, showing the phases present.

unreacted Al. The grain size difference between the G2cBN and the G20cBN composites is apparent.

3.2. Hardness

Fig. 3a and b shows the results of the Vickers hardness measurements of the sintered polycrystalline cBN–Al composites at room temperature plotted against the grain size of the cBN hard phase and against sintered binder content. The hardness values show that the G2cBN15 has the highest hardness of 40 ± 1.2 GPa, while the G20cBN25 containing binders the lowest hardness of 15.6 ± 0.4 GPa. The hardness of the PcBN–Al composites decreases with increasing cBN grain size and increasing binder content.

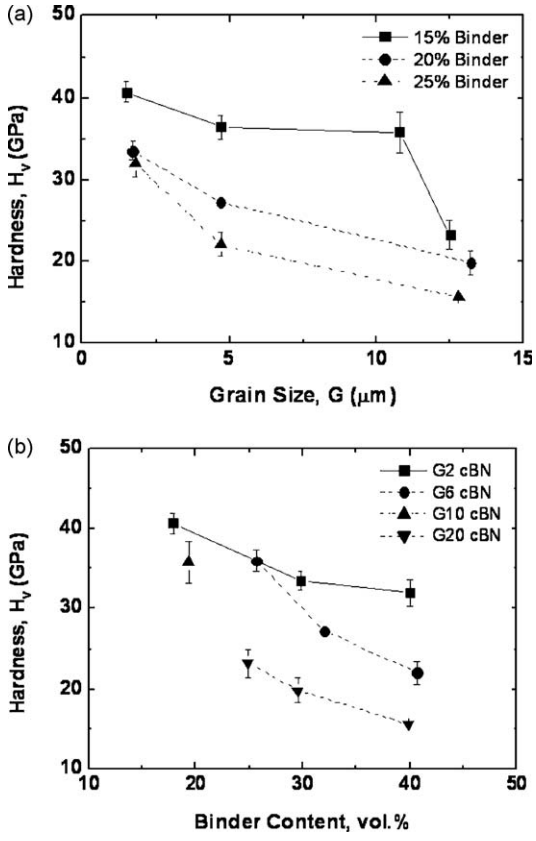

Fig. 3. Hardness of PcBN–Al composite as function of cBN grain size: (a) dependence on grain size of cBN and (b) dependence on binder content.

The hardness is determined by the amount of the ultra-hard cBN phase. At lower content of binder phases there are more cBN–cBN contacts thus leading to higher hardness. The hardness decreases with increasing cBN grain size in agreement with the Hall–Petch relationship [21] (i.e. $H \propto 1/\sqrt{d}$).

The hardness of the PcBN–Al composite materials produced in this work is in the same range as the hardness published by other authors. The hardness of single crystal cBN grains is 50 GPa [2] and Amborite [1] (Element Six (Pty), Ltd.), a commercially produced material which contains cBN of 90 wt.% with aluminium and other metals as the binder phase, has a Knoop hardness of 31.5 GPa. Rong and Fukunaga [9] measured the Knoop hardness of their cBN–Al composites to lie between 15 and 35 GPa.

3.3. Fracture toughness and strength

The results of the SEVNB fracture toughness measurements are summarized in Table 2. Fig. 4a and b showing the fracture toughness as a function of the grain size of the cBN hard phase and sintered binder content. The mean values and standard deviations of the fracture toughness values were calculated without outliers (data points differing by at least 0.65 MPa $m^{1/2}$ were considered as outliers). The mean values of the fracture toughness of all composites are in the range between 6.6 and 8.0 MPa $m^{1/2}$.

Considering the effect of grain size of cBN the highest fracture toughness values were achieved with grain sizes >10 μm and binder contents of 15–20 vol.%. Fracture toughness increases with increasing grain size, up to $\sim$10 μm, with the batches containing 15 and 20 vol.% binder. With 25% binder content the fracture toughness is lower, and there is no significant grain size dependence of the fracture toughness detected. Considering the binder content the fracture toughness of the batches with 6 and 20 μm cBN grain size does not show a significant dependence of binder content at 15–20 vol.%, but decreases at 25 vol.%. The batches with 2 μm grain size show a slight increase of fracture toughness with

Table 2
Fracture toughness of the PcBN–Al composite materials.

Sample	No. of tests (outliers)[a]	K_{Ic} (MPa $m^{1/2}$)
G2cBN15	4 (1)	6.6 ± 0.1
G2cBN20	5 (1)	6.9 ± 0.3
G2cBN25	5 (0)	7.1 ± 0.2
G6cBN15	5 (1)	7.6 ± 0.3
G6cBN20	5 (0)	7.6 ± 0.3
G6cBN25	4 (0)	7.0 ± 0.3
G10cBN15	5 (0)	8.0 ± 0.1
G20cBN15	4 (0)	7.9 ± 0.2
G20cBN20	5 (1)	8.0 ± 0.1
G20cBN25	5 (0)	7.0 ± 0.1

[a] If a value differs by $\geq$0.65 MPa $m^{1/2}$ from the next nearest value it is considered as outlier and not taken into account.

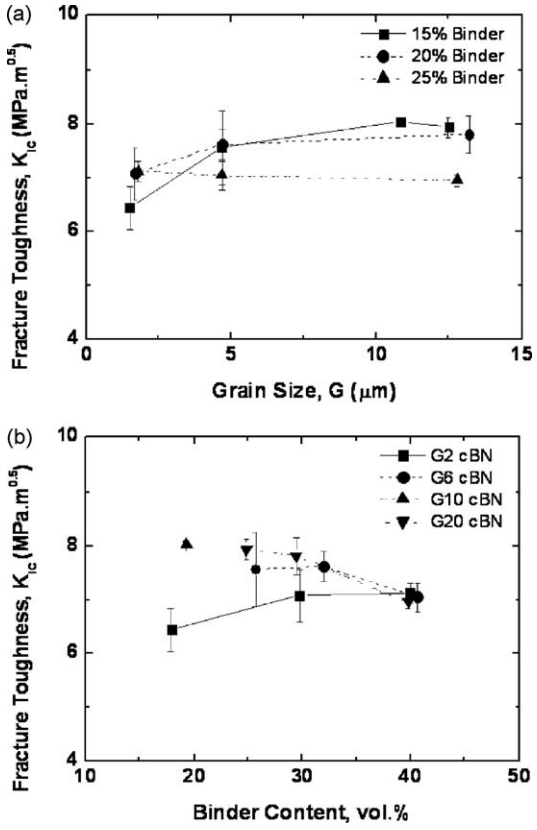

Fig. 4. Fracture toughness of the PcBN–Al composite materials: (a) dependence on grain size of cBN and (b) dependence on binder content.

increasing binder content from 15 and 20 vol.%. However, this is at a low level.

The measured fracture toughness values are above those reported for cBN materials of 3–6 MPa m$^{1/2}$ [1], and are also mostly higher than those of Amborite, a commercial 'Element Six' material of PcBN with a mostly AlN binder phase, with a fracture toughness of 6.4 MPa m$^{1/2}$ [1]. It should be noted that properties of ceramic materials are highly sensitive to the method employed and thus a direct comparison of these results is difficult as the test methods differ.

Fig. 5 shows a crack propagating through a G20cBN25 composite material and fracture surfaces of fracture toughness samples of G2cBN15 and of G20cBN25. From the crack path in Fig. 5a, a tendency of predominant crack propagation in the binder phase might be deduced; this is valid at least for that composition and microstructure.

The high fracture toughness is substantiated by crack deflection/bridging observed during crack propagation (Fig. 5). Crack deflection can lead to a small increase in the crack tip toughness, for example as determined for whisker-reinforced alumina [22], but mainly aids in setting up efficient crack bridges leading to *R*-curve behavior [23], further unreacted aluminium will lead to a small contribution by ductile bridging. However, the difference in the fracture toughness of materials with and without residual Al is not significant. Therefore this mechanism (ductile bridging) is not a dominant one.

The results of bending strength measurements are summarized in Table 3, including the 90% confidence intervals. The

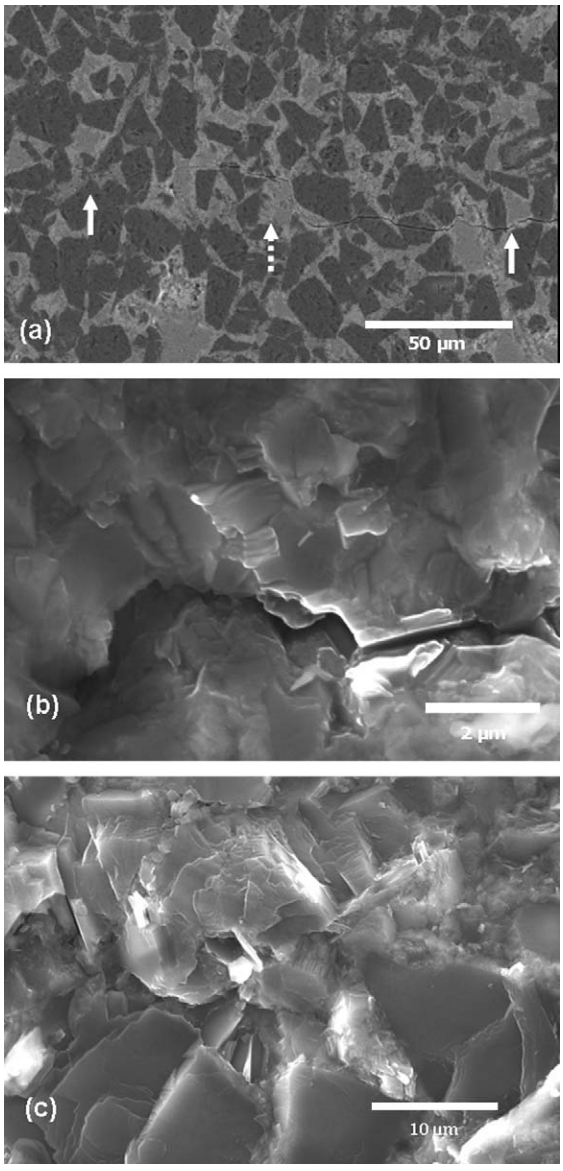

Fig. 5. Crack propagation in fracture toughness tests: (a) fracture path on polished surface of G20cBN25 sample exhibiting slightly predominant crack propagation in the binder phases, (b) fracture surface of G2cBN15 exhibiting crack propagation through the binder phases, and (c) fracture surface of G20cBN25 exhibiting crack propagation through the binder phases.

Table 3
Characteristic strength σ_o, Weibull modulus *m* and respective 90% confidence intervals (c.i.) of the PcBN–Al composite materials.

Sample	σ_o (MPa)	90% (c.i.)	*m*	90% (c.i.)
G2cBN15	390	373–409	9.8	6.6–12.5
G2cBN20	433	407–460	7.0	4.8–8.8
G2cBN25	445	427–462	10.7	7.4–13.5
G6cBN15	409	382–439	6.1	4.2–7.8
G6cBN20	395	384–406	15.7	10.7–19.9
G6cBN25	429	418–440	16.2	11.2–20.5
G10cBN15	454	446–462	24.0	16.6–30.3
G20cBN15	396	386–406	16.6	11.5–21.0
G20cBN20	355	349–361	24.9	17.2–31.4
G20cBN25	390	381–398	19.9	13.6–25.2

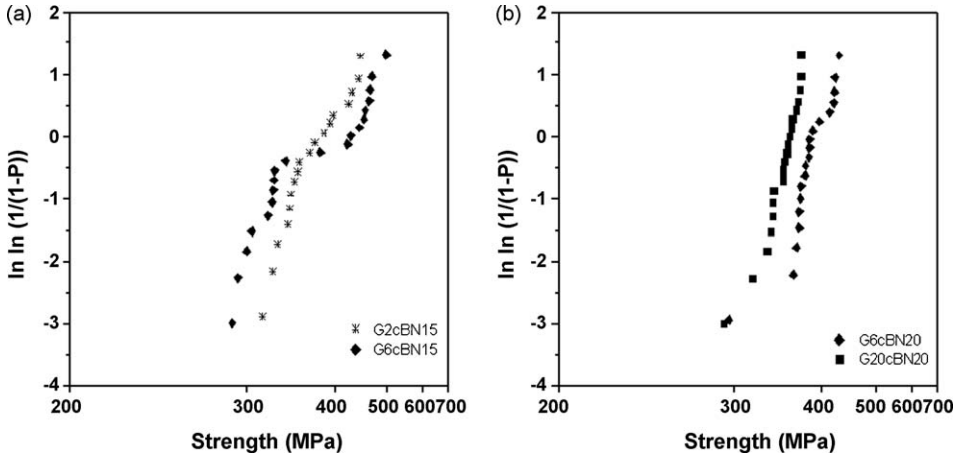

Fig. 6. Weibull distributions of bending strength data: (a) with low Weibull moduli, 6–10, batches G2cBN15, G6cBN15 and (b) with Weibull moduli of 15 and 25, batches G6cBN20 and G20cBN15.

characteristic strength values of the cBN composite materials are in a narrow range between 355 and 454 MPa . They are much lower than values reported for PcBN materials of up to 800 MPa [1]. The range of the Weibull moduli between 6.1 and 24.9 is quite large. Considering the strength distributions of the batches with low Weibull moduli more closely, the strength data of these batches display signs of bimodal distributions; whereas strength data of the batches with high m values seem likely to belong to monomodal distributions (cf. Fig. 6). However, the considerations about the attribution of the data to bi- and monomodal distributions suffer from the quite small number of test specimens; the scatter of the data may have multiple reasons [24].

Fig. 7a and b presents the variation of the characteristic strength values, σ_o, as function of the grain size of the cBN phase and of the sintered binder content. The strength appears to decrease with increasing grain size, at least with the batches with 20 and 25 vol.% binder content. This decrease in strength with grain size is a common feature for most ceramics [25] and related to the size of the initial flaw as related to the grain size [26]. With 15 vol.% binder there is no clear trend. Also, there are no clear trends of strength dependence on binder content.

Crack initiating flaws were characterized for 10–15% of the tested specimens of each batch (in total 200 specimens were tested), from specimens of low, of medium and of high strength. In most cases the crack initiating flaws were clearly identified. The identified flaws were quite large, having a maximum diameter of 100–500 μm (see Fig. 8). These large flaws appear to be responsible for the low strength (which is atypical for commercial materials), particularly since the fracture toughness is superior to other PcBN materials.

If we assume that the measured fracture toughness, K_{Ic}, is close to the fracture toughness relevant for fracture of bend bars, the size of a crack initiating flaw can be calculated for a definite strength value σ_f according to [27]:

$$a = \left(\frac{K_{Ic}}{\sigma_f \cdot Y}\right)^2 \quad (1)$$

In Eq. (1), a is the radius of the flaw at instability and the defect shape parameter Y is taken as $Y = \sqrt{\pi}/2$ for penny-shaped cracks. Crack sizes computed using Eq. (1) compare favorably with actually measured defect sizes on fracture surfaces (see Fig. 9).

The failure initiating flaws were often found to be elongated with aspect ratio from 1.5 to 5, see examples in Fig. 8, with the largest diameter always oriented perpendicular to the specimen length (i.e. perpendicular to direction of loading during

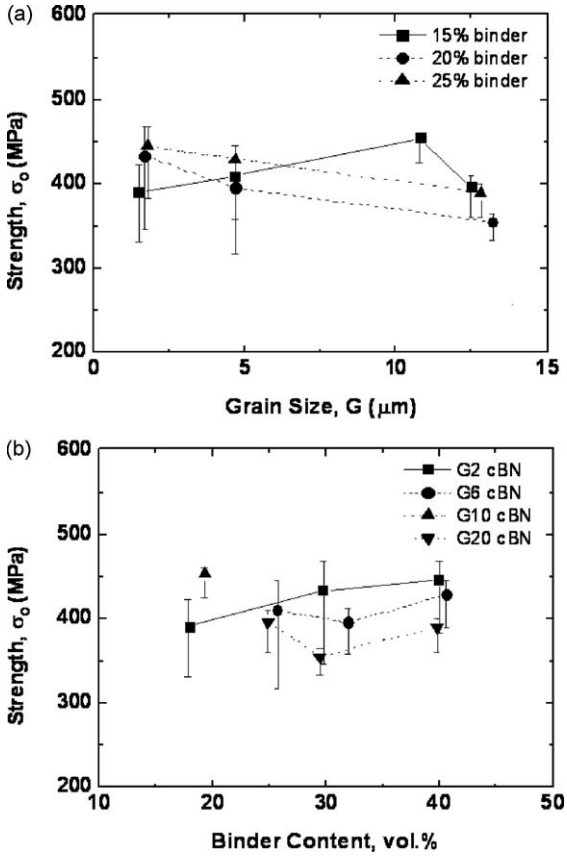

Fig. 7. Strength of PcBN–Al composite materials with scatter bands covering 63% of strength values, which is equivalent to the range covered by the standard deviation in Gaussian statistics: (a) dependence on cBN grain size and (b) dependence on binder content.

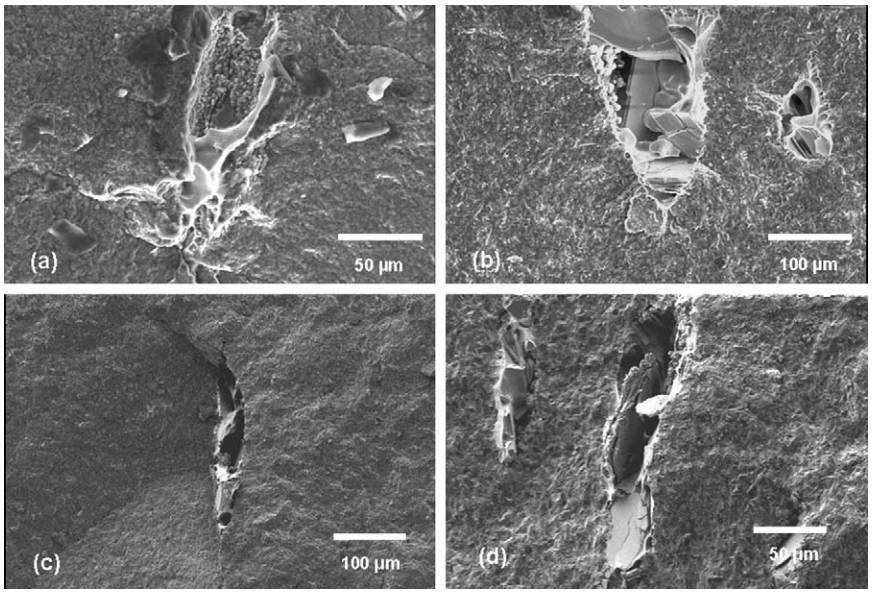

Fig. 8. Typical flaws from low and high strength samples. (a) Low strength flaw with features of ductile fracture, sample from batch G2cBN15. (b) Low strength flaw with very large grains, sample from batch G6cBN20. (c) High strength flaw, sample from batch G2cBN25. (d) High strength flaw, sample from batch G6cBN25.

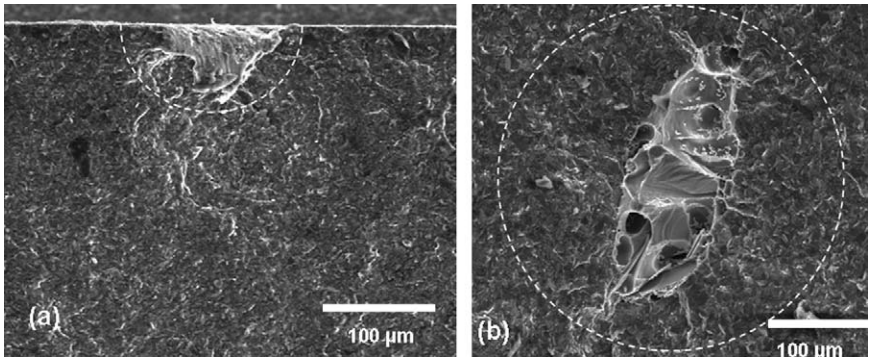

Fig. 9. Model crack size calculated from fracture toughness and strength limiting flaws: (a) G6cBN15, K_{Ic} = 7.6 MPa $m^{1/2}$, σ_f = 497 MPa, and (b) G10cBN15, K_{Ic} = 8.0 MPa $m^{1/2}$, σ_f = 378 MPa.

manufacture). They either exposed features of ductile rupture or contained very large grains. These characteristics were irrespective of the location of the flaws, in the bulk or at the tensile surface of the specimens. They clearly point to deficiencies in powder processing. The flaws exhibiting ductile fracture originated from large particles or agglomerates of the binder pools some with unreacted aluminium as proven by EDX analysis.

The microstructure and size of the flaws indicate not intensive enough deagglomeration and homogenization of cBN and binder during powder processing. The high aspect ratio and parallel orientation of the flaws point out that they originate before the HPHT step and underscore the deficiencies in powder processing.

The poor correlation of strength and cBN grain size and binder content is presumably due to the very broad scatter of flaw sizes and its weak correlation to processing of the individual material batches.

The scatter of strength of the different materials differs significantly as witnessed by the range of *m* values of 6–25. The deviation of some of the strength data from a monomodal distribution is a major reason. A clarification would need a thorough correlation of strength values to the kind and size of the crack initiating flaws. As stated above, this is out of the scope of the present study.

4. Summary and conclusions

The hardness of the PcBN materials prepared with Al binder is high as expected due to the hard cBN phase. It decreases with increasing cBN grain size and increasing binder content.

Fracture toughness is high compared to other PcBN materials. Fracture toughness depends on grain size and binder content, but to a much lesser extent than hardness and has a less clear tendency. The cracks propagate mostly through the binder phase; there are signs of crack deflection and crack bridging. Crack deflection may be associated with residual stresses in the constituent phases.

The high fracture toughness values are in good correlation with the observed sizes of fracture origins and the corresponding strength values.

Strength values are low compared to literature values. They show no clear dependence on grain size and binder content. Both facts are due to very large strength limiting flaws.

Acknowledgements

Thanks to the following organizations for funding and sponsorship; National Research Foundation (NRF), Centre of Excellence (CoE) in Strong Materials and Element Six (Pty) Ltd. Thanks to Element Six (Pty) Ltd. for the use of their HPHT facilities and the Institute of Materials Science, Technische Universität Darmstadt for the material testing.

References

[1] R. Riedel, Handbook of Ceramic Hard Materials, Wiley-VCH, 2002.
[2] J. Haines, J.M. Leger, G. Bocquillon, Synthesis and design of superhard materials, Annual Review Materials Research 31 (2001) 1–23.
[3] T.K. Harris, E.J. Brookes, C.J. Taylor, The effect of temperature on the hardness of polycrystalline cubic boron nitride cutting tool materials, International Journal of Refractory Metals and Hard Materials 22 (2–3) (2004) 105–110.
[4] T. Taniguchi, M. Akaishi, S. Yamaoka, Sintering of cubic boron nitride without additives at 7.7 GPa and above 2000 °C, Journal of Materials Research 14 (1) (1999) 162–169.
[5] E. Benko, P. Klimczyk, S. Mackiewicz, T.L. Barr, E. Piskorska, cBN–Ti_3SiC_2 composites, Diamond and Related Materials 13 (3) (2004) 521–525.
[6] Ltd. Sumitomo Electrical Industries, US patent 4 334 063. Patent (1982).
[7] R.H. Wentorf, W.A. Rocco, Japanese patent appl. no. 65393. Patent (1972).
[8] J.C. Walmsley, A.R. Lang, A transmission electron-microscope study of a cubic boron nitride-based compact material with AlN and AlB_2 binder phases, Journal of Materials Science 22 (11) (1987) 4093–4102.
[9] X.Z. Rong, O. Fukunaga, Sintering of cubic boron nitride with added aluminium at high pressure and high temperatures, Diamond and Related Materials B 14 (1994) 1455–1458.
[10] E. Benko, J. Morgiel, T. Czeppe, BN sintered with Al: microstructure and hardness, Ceramics International 23 (1) (1997) 89–91.
[11] X.Z. Rong, T. Yano, TEM investigation of high-pressure reaction-sintered cBN–Al composites, Journal of Materials Science 39 (14) (2004) 4705–4710.
[12] Y.C. Zhao, M.Z. Wang, Cubic BN sintered with Al under high temperature and high pressure, Chinese Physics Letters 24 (8) (2007) 2412–2414.
[13] Y. Li, S. Li, R. Lv, J. Zhang, J. Wang, F. Wang, Z. Kou, D. He, Study of high-pressure sintering behavior of cBN composites starting with cBN–Al mixtures, Journal of Materials Research 23 (9) (2008) 2366–2372.
[14] T. Wada, N. Yamashita, Formation of cBN–Al films by ion-beam assisted deposition, Journal of Vacuum Science and Technology A 10 (3) (1992) 515–520.
[15] R. Moon, K. Bowman, K. Trumble, J. Rödel, A Comparison of *R*-curves from SEVNB and SCF fracture toughness test methods on multilayered alumina–zirconia composites, Journal of the American Ceramics Society 83 (2) (2002) 445–447.
[16] ASTM C 1161-02c, Standard test method for flexural strength of advanced ceramics at ambient temperatures, 2002.
[17] R. Damani, R. Gstrein, R. Danzer, Critical notch-root radius effect in SENB-S fracture toughness testing, Journal of the European Ceramic Society 16 (1996) 695–702.
[18] European Standard EN843-1: Advanced Technical Ceramics – Monolithic Ceramics – Mechanical Properties at Room Temperature—Part 1: Determination of Flexural Strength, 1995.
[19] European Standard EN843-5: Advanced Technical Ceramics – Monolithic Ceramics – Mechanical Properties at Room Temperature—Part 5: Statistical Evaluation of Strength Values, 1997.
[20] D.R. Thoman, C.J. Bain, C.E. Antle, Interferences on the parameters of the Weibull distribution, Technometrics 11 (3) (1969) 445–460.
[21] R.W. Rice, C. Wu, F. Boichelt, Hardness–grain-size relations in ceramics, Journal of the American Ceramics Society 77 (10) (1994) 2539–2553.
[22] J. Rödel, E.R. Fuller Jr., B.R. Lawn, In-situ observations of toughening processes in alumina reinforced with silicon carbide whiskers, Journal of the American Ceramics Society 74 (12) (1991) 3154–3157.
[23] J. Rödel, Interaction between crack deflection and crack bridging, Journal of the European Ceramics Society 10 (3) (1992) 143–150.
[24] R. Danzer, P. Supancic, J. Pascual, T. Lube, Fracture statistics of ceramics – Weibull statistics and deviations from Weibull statistics, Engineering Fracture Mechanics 74 (2007) 2919–2932.
[25] J. Seidel, N. Claussen, J. Rödel, Reliability of alumina: effect of grain size, Journal of the European Ceramics Society 15 (1995) 395–404.
[26] A. Zimmermann, M. Hoffman, B.D. Flinn, R.K. Bordia, T. Chuang, E.R. Fuller Jr., J. Rödel, Fracture of alumina with controlled pores, Journal of the American Ceramics Society 81 (9) (1998) 2449–2457.
[27] D. Munz, T. Fett, Ceramics: Mechanical Properties, Failure Behaviour, Materials Selection, Springer, 2001.